Journal of Molecular Modeling (2021) 27: 270
https://doi.org/10.1007/s00894-021-04889-9

ORIGINAL PAPER

Defective GaAs nanoribbon–based biosensor for lung cancer biomarkers: a DFT study

Tarun Tarun[1] · Paramjot Singh[1] · Harmandar Kaur[2] · Gurleen Kaur Walia[3] · Deep Kamal Kaur Randhawa[2] · B. C. Choudhary[4]

Received: 6 July 2021 / Accepted: 19 August 2021 / Published online: 30 August 2021

Abstract

Density functional theory-based first-principles investigation is performed on pristine and mono vacancy induced GaAs nanoribbons to detect the presence of three volatile organic compounds (VOCs), aniline, isoprene and o-toluidine, which will aid in sensing lung cancer. The study has shown that pristine nanoribbon senses all three analytes. For the pristine structure, we observe decent adsorbing parameters and the bandgap widens after the adsorption of analytes. However, the introduction of the carrier traps induced by defect causes deep energy wells that vary the electrical properties as indicated in the bandgap analysis of GaAs, wherein adsorption of aniline and o-toluidine reduces the bandgap to 0 eV, making the structure highly conductive in nature. The adsorption energies of defect-induced nanoribbon are more as compared with the pristine counterpart. Nonetheless, the introduction of defects has improved the sensitivity further.

Keywords Nanoribbons · Lung cancer · Biomarker · Biosensor · Density functional theory (DFT) · Gallium arsenide

Introduction

Of the innumerous diseases that affect humans, lung cancer accounts for more than 2.1 million infected people annually. The infected people have a bleak survival rate since the early-stage diagnosis of this disease is very rare. Although there are some techniques for the diagnosis, such as lung biopsy, chest X-ray scan and bronchoscopy, these are hazardous and expensive. Even with sophisticated treatment such as surgical resection, the stage 3 cancer patient has only a 30% survival rate [1]. In lung cancer, the diseased cells attack the host's living cells, causing a biochemical reaction forming volatile organic compounds (VOCs). These VOCs are present in the exhalation of the infected person. Some common and prominently present biomarkers exhaled by an infected person are aniline, isoprene and o-toluidine [2]. The detection of these biomarkers in-breath is a vital early-stage diagnostic step of this dangerous disease. The detection of biomarkers for disease diagnosis was first proposed by Pauling et al. [3]. With the detection of VOCs, the information about the biological reactions inside the human body can be revealed, which helps in disease diagnosis. Nanomaterials can play a pivotal role in the detection of biomarkers. Various studies in literature corroborate that nanomaterials are excellent in detecting gases and biomolecules [4–10]. Owing to the excellent electrical and transport properties of 2-dimensional nanomaterials, such as graphene [11–15], silicene [16–22], ZnO nanoribbons [23–25] and germanene [26–29], they are emerging as promising candidates in the field of sensing [30]. GaAs nanoribbon is a one-dimensional nanomaterial with unique electrical, mechanical and optical properties [31]. In particular, GaAs has potential applications in photovoltaic [32], electronic and optoelectronic [32] devices. However, not much research is done on GaAs nanoribbon for a vital application of sensing different analytes. Monolayer GaAs have feature-rich energy bands, mainly due to the significant buckled structure, sp^3 bonding

✉ Gurleen Kaur Walia
gurleen.24800@lpu.co.in

[1] Electrical and Computer Engineering Department, Concordia University, Montreal H3G 1M8, Canada

[2] Department of Electronics and Communication Engineering, Guru Nanak Dev University, Regional Campus, Jalandhar, Punjab, India

[3] School of Electronics and Electrical Engineering, Lovely Professional University, Phagwara, Punjab, India

[4] Applied Science Department, National Institute of Technical 'Teachers' Training and Research (NITTTR), Chandigarh, India

and spin-orbital coupling (SOC) [33]. According to the first-principles calculations, monolayer GaAs possess the buckled hexagonal structure, multi-orbital chemical bonding and significant spin-orbital coupling, which is expected to induce the rich electronic properties and diverse magnetic quantization in the presence/absence of electric fields [31, 34]. Sahin et al. [35] determined that the two-dimensional graphene-like structures of group III-As (BAs, GaAs and InAs) are stable semiconductors using first principles.

In this work, armchair GaAs nanoribbons (both pristine and defect induced) have been studied for the vital application of detecting the VOCs in the exhalation of a person infected with lung cancer. The VOCs under analysis are aniline (C_6H_7N), isoprene (C_5H_8) and o-toluidine (C_7H_9N) molecules. The basis of this study is to analyze the electrical, optical and transport properties upon the adsorption of the identified VOCs on the surface engineered and pristine GaAs nanoribbon. The induced defects on GaAs nanoribbon cause trap states that are highly localized and carriers trapped in these states cannot move easily in the energy bandgap, causing a variation in the conductivity. The surface defects may be possible trap sites for the charge carriers. The trapping of the charge carriers promotes the counter charge carriers reaching the surface. Also, there are possibilities of frequent electron–hole recombination at these trap sites. For the complete characterization of the considered VOCs adsorbed GaAs nanoribbon, the density functional theory (DFT) and non-equilibrium Green's function (NEGF)–based first-principles investigation has been performed to calculate the electronic and transport properties of the VOCs nanosensing application for early-stage lung cancer diagnosis.

Computational studies

The calculations are performed on the Virtual NanoLab Atomistix Tool Kit (VNL-ATK) simulation package [36]. In this work, the electronic properties, viz., the bandstructure, density of states, electron density, transport properties including I-V characteristics, transmission eigenstates and optical spectrum, have been calculated and analyzed. Armchair GaAs nanoribbon with a width of $n=6$ is analyzed. The structures were edge passivated by hydrogen atoms to passivate the dangling bonds [20]. The GaAs bond length is measured to be 2.409 Å, as shown in Fig. 1.

The ideal lattice parameter for 1D GaAs primitive cell is 4.00 Å. DFT-based NEGF calculations have been performed. Generalized gradient approximation (GGA) along with Perdew-Burke-Ernzerhof (PBE) and double zeta polarized (DZP) set is used as exchange–correlation function and basis set, respectively. The density mesh cutoff frequency and electron temperature are 80 Hartree and 300 K, respectively. The force and stress tolerance is set to be 0.05 eV/Å and 0.05 eV/Å^3, respectively. *K*-point sampling is set to be $1\times1\times7$ for optimization and $1\times1\times99$ for the rest of the calculations. The adsorbent molecule is placed approximately at a vicinity of 3 Å from the GaAs nanoribbon. All the complexes of the base material and analytes are allowed to fully relax using geometry optimization before calculating the characteristic properties. For calculating the transport properties, a two-probe model of the structure is formed and has been designed, as shown in Fig. 2. Hence, a two-probe model consists of

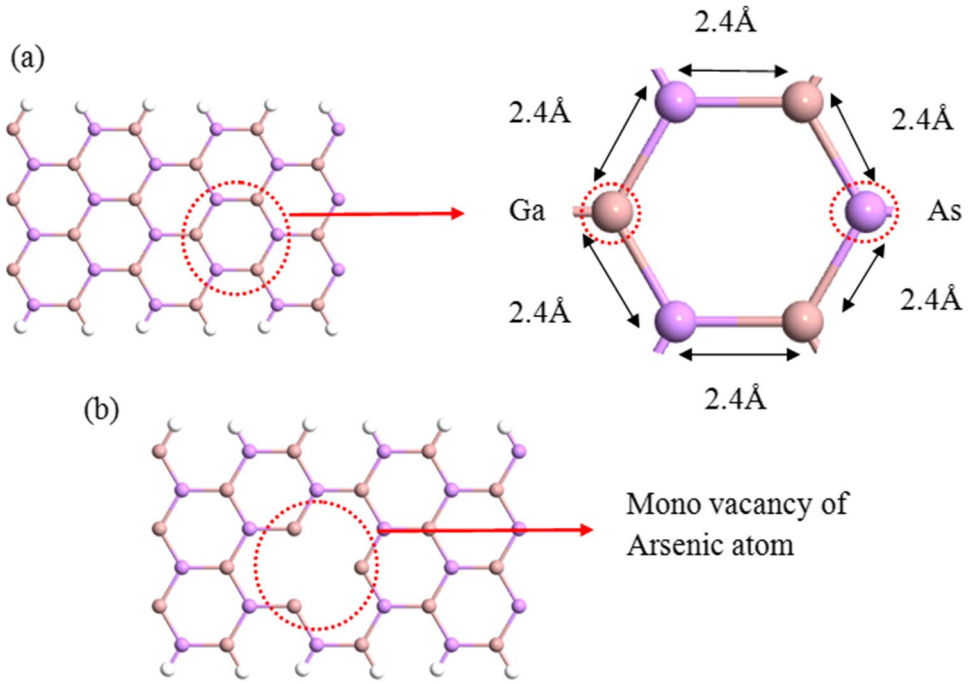

Fig. 1 Structure of **a** pristine and **b** defective GaAs nanoribbon

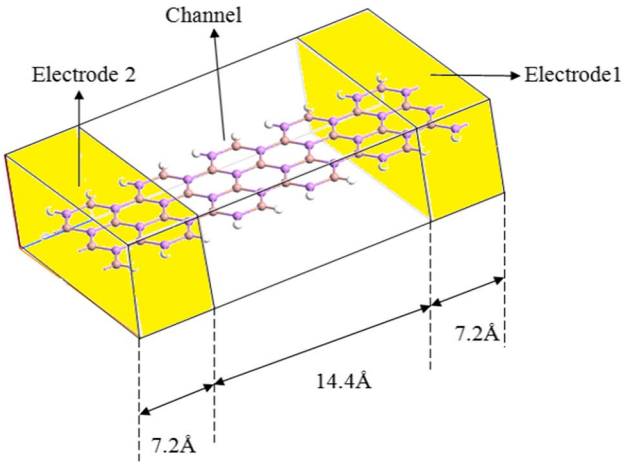

Fig. 2 Two-probe model-based GaAs nanoribbon device

two electrodes and a scattering region. Both the electrodes have lengths of 7.2 Å, and the scattering region was measured to be 14.4 Å.

Results and discussion

After the optimization, both pristine and defective nanoribbons, formed van der Waals interactions with all the three VOC analytes. Generally, for a nanoribbon, two adsorption mechanisms, physisorption and chemisorption, prevail. Physisorption means there is no physical contact between the surface and the analyte; they are only held together by weak van der Waals forces. On the other hand, chemical interactions involve the formation of strong chemical bonds. Also, the formation of the chemical bonds between substrate and analyte generally distorts the geometry of substrate and hence this type of sensing material is suitable for one-time use. Figures 3 and 4 show the most favourable positions of

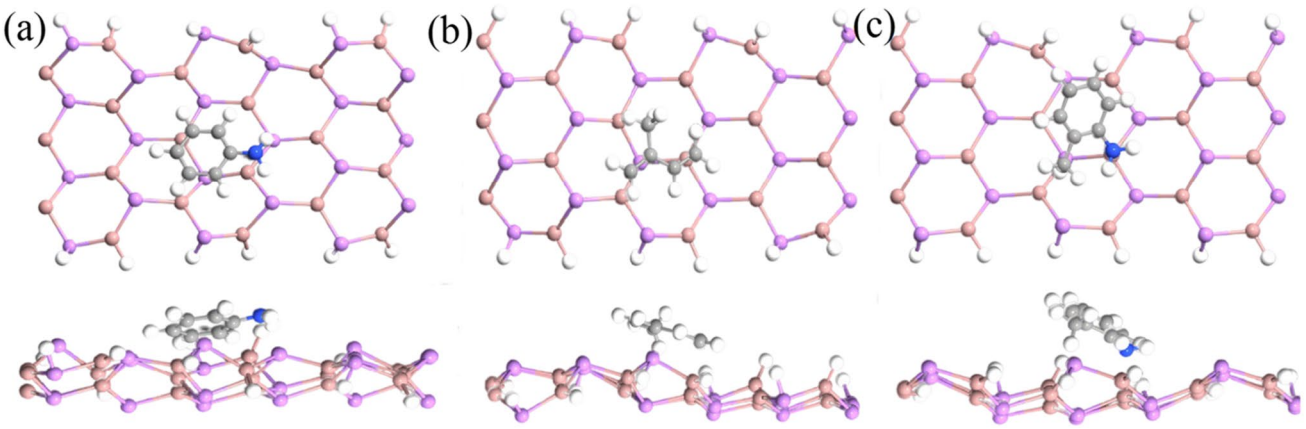

Fig. 3 Pristine GaAs nanoribbon with adsorbed **a** aniline, **b** isoprene and **c** o-toluidine, respectively

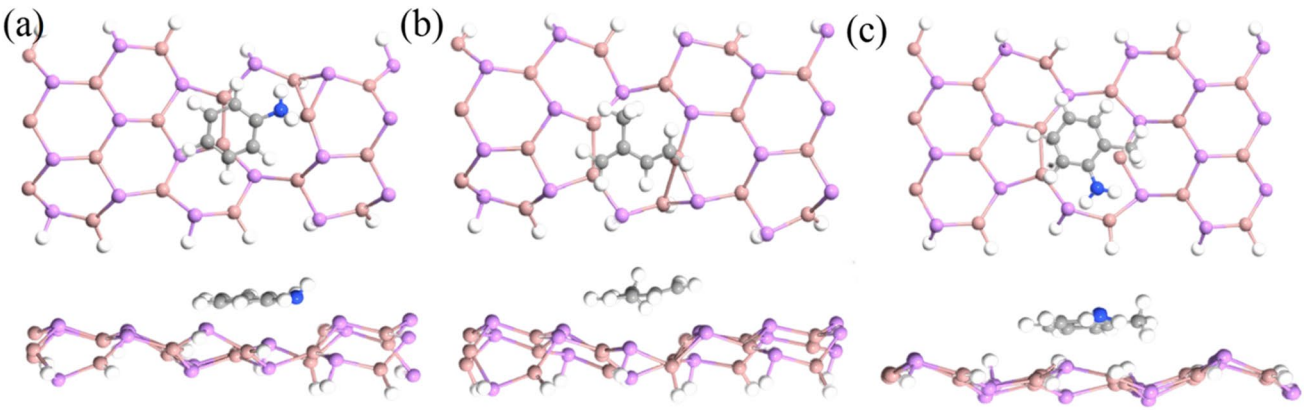

Fig. 4 Defective GaAs nanoribbon with adsorbed **a** aniline, **b** isoprene and **c** o-toluidine, respectively

the pristine and defective nanoribbons with the adsorbed analytes, respectively.

The adsorption of the biomarker molecules changes the buckling height (in Figs. 3 and 4) and geometry of the clar's structure by the formation of the triangle (in Fig. 4a, b). This change in the periodic potential of nanoribbon increases the generation of the phonon in the lattice and results in strong interaction between the charge carriers (electrons) and phonons which deteriorate the transport properties of the material, which are discussed with current characteristics in the latter part of this section. Moreover, in the comparison of biomarker-adsorbed GaAs nanoribbon (Fig. 4) with biomarker-adsorbed defective GaAs nanoribbon (Fig. 5), the defective one shows less distortion in the lattice as compared to the pristine GaAs nanoribbon biomarker complex, which confirms the better transport properties of biomarker-adsorbed defective GaAs nanoribbon.

Dangling bonds are passivated with the hydrogen to nullify its effect on the adsorption of the biomarkers.

To get the intuitive perception about the binding of the biomarker with the host material, adsorption energy is calculated. The more negative the value of adsorption energy is, the stronger the interaction and the more is the charge transfer. The adsorption energy is calculated as:

$$E_{AD} = E_{(GaAs+VOC)} - E_{(GaAs)} - E_{(VOC)} \quad (1)$$

E_{AD} represents adsorption energy, $E_{(GaAs+VOC)}$ represents the energy of nanoribbon and analyte combined, $E_{(GaAs)}$ represents the energy of nanoribbon and $E_{(VOC)}$ represents the energy of analyte. Table 1 summarises the adsorption

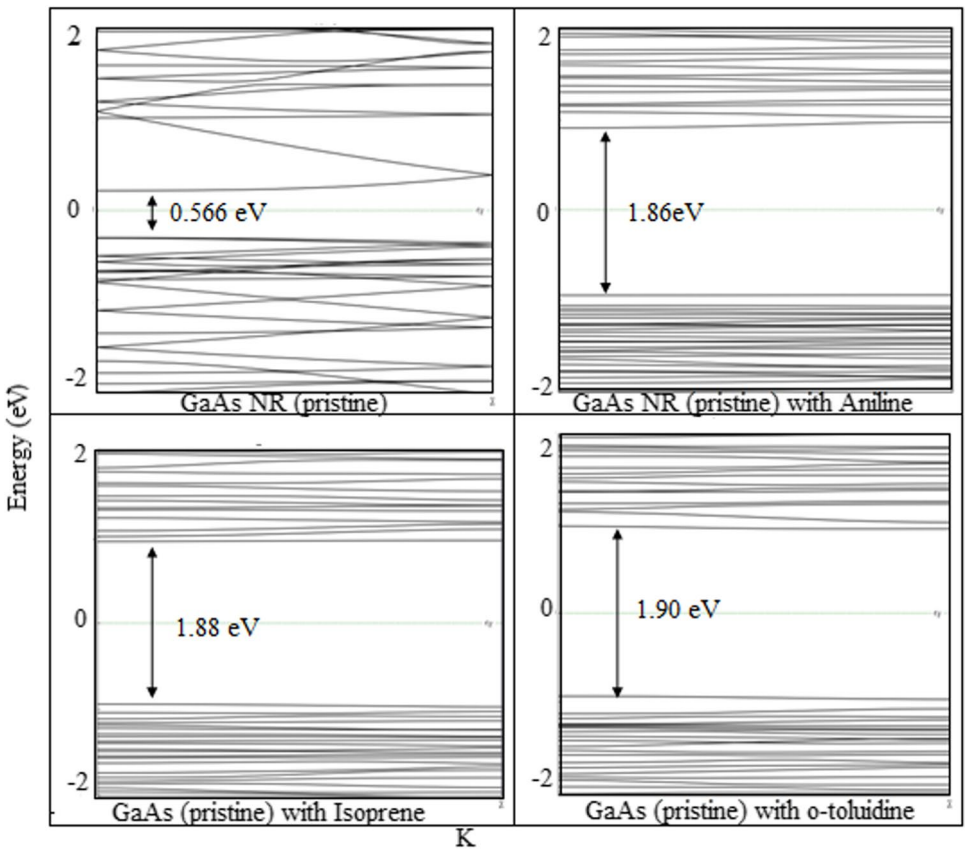

Fig. 5 Band structures of pristine GaAs nanoribbon with all three VOC analytes

Table 1 Adsorption energies of pristine and defective GaAs with all three VOC analytes

Configuration	$E_{(GaAs+VOC)}$ (eV)	$E_{(GaAs)}$ (eV)	$E_{(VOC)}$ (eV)	E_{AD} (eV)
Pristine GaAs with aniline	− 90,952.4	− 89,568.7	− 1376.13	− 7.61
Pristine GaAs with isoprene	− 90,522.8	− 89,568.7	945.89	− 8.15
Pristine GaAs with o-toluidine	− 91,149	− 89,568.7	− 1567.89	− 12.96
Defective GaAs with aniline	− 8806.64	− 86,680.5	− 1376.13	− 10.50
Defective GaAs with isoprene	− 87,638.1	− 86,680.5	945.89	− 12.96
Defective GaAs with o-toluidine	− 88,261.5	− 86,680.5	− 1567.89	− 12.91

energies obtained for pristine and defective GaAs nanoribbon with the adsorbed VOC analytes.

GaAs crystal is a direct bandgap material, and so its quasi-one-dimensional nanoribbon with the bandgap of 0.556 eV in its pristine form. With the introduction of the defect, the bandgap reduces to 0.3 eV and the material changes from intrinsic to a p-type semiconductor by moving the Fermi level to valence band maxima (VBM). It occurs because of the trapping energy states that occur near the Fermi level. The formation of trapping states depends upon the perturbation in the Hamiltonian/ potential of the superlattice of the nanoribbon. This fluctuation of the potential changes the energy eigenvalues and affirms the permutation of the energy states, which leads to the formation of energy states in the forbidden energy band of pristine nanoribbon, which are known as trapping states. The release of the trapped carriers is dependent on the thermally activated process.

For the pristine GaAs nanoribbon, the bandgap increases to 1.86 eV, 1.88 eV and 1.9 eV after aniline, isoprene and o-toluidine adsorptions, respectively. It can be seen that the pristine GaAs substrate is an intrinsic semiconductor after the adsorptions of all three VOCs. The bandgap reduces to 0 eV on aniline adsorption for the defective GaAs nanoribbon, making the complex of GaAs-aniline metallic. Despite the fact that there is no overlapping of conduction and valence band, the Aniline-GaAs nanoribbon complex shows metallic nature because the VBM crossed the Fermi level as shown in Fig. 6, which signifies the half-filled nature of VBM, which is one of the characteristic natures of metals.

Similar phenomena have been observed in the case of o-toluidine-adsorbed GaAs nanoribbons. However, the unfilled electron region in the o-Toluidine case is the opposite of aniline. Furthermore, on adsorption of isoprene, the bandgap is 0.7 eV and shows n-type semiconductor behaviour. Table 2 summarises the obtained bandgaps of all the considered variants, including the intrinsic materials.

The density of states represents the number of states available to be occupied by the electrons. The DOS has same value corresponding to the bandstructure; hence, it is one of the most essential parameters in analyzing the adsorption behaviour accompanied by bandstructure. Figure 7 shows the DOS comparison of pristine GaAs with the three VOC analytes. It can be seen clearly that after the adsorption of the analytes, the free states are occupied by the carriers, and the change can be seen through the difference between the DOS level in all three cases. Figure 8 presents the DOS comparison of defective nanoribbon with all three analytes. Before discussing the results of the adsorption on defective nanoribbon, it should be clear that by inducing a defect, trapping states are formed near the Fermi level as observed in Fig. 8. The defect-induced nanoribbon shows the slowing of the charges as they move through the semiconductor proportional to the

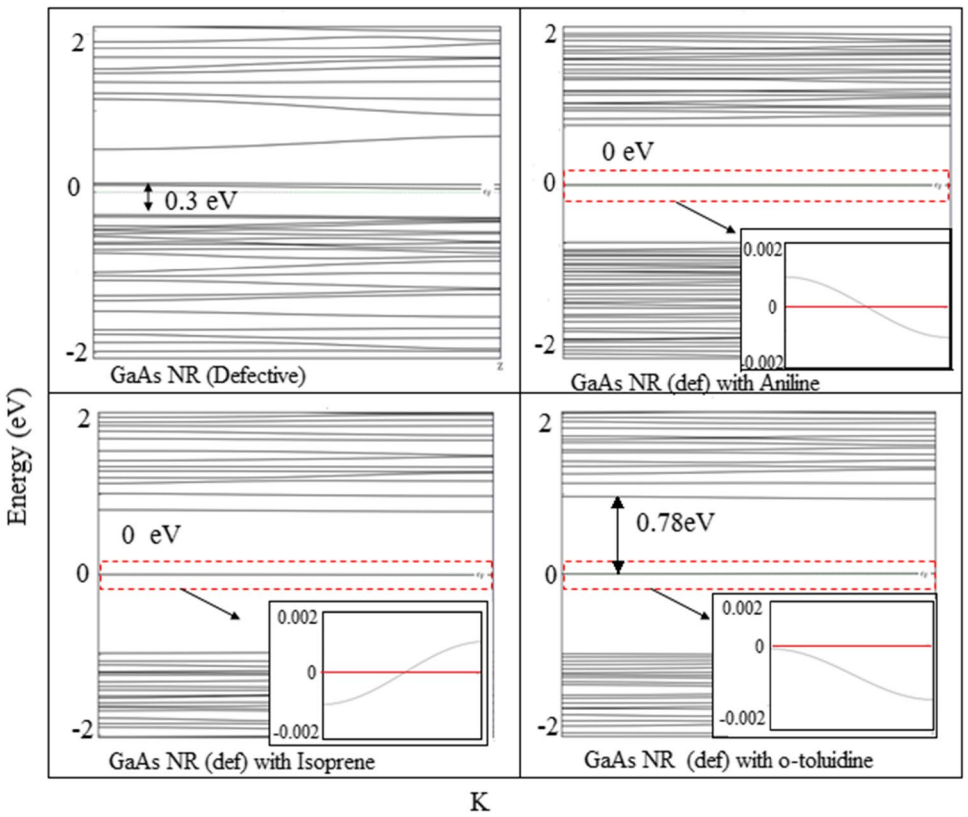

Fig. 6 Band structures of defective GaAs nanoribbon with all three VOC analytes

Table 2 Bandgaps of pristine and defective GaAs nanoribbon with respective analytes

Configuration	Band gap (eV)	Valence energy level (eV)	Conduction energy level (eV)	Material type
Pristine GaAs	0.52	−0.25	−0.25	Semiconductor (I)
Pristine GaAs with aniline	1.86	−0.94	0.90	Semiconductor (I)
Pristine GaAs with isoprene	1.88	−0.94	0.94	Semiconductor (I)
Pristine GaAs with o-toluidine	1.9	−0.93	0.94	Semiconductor (I)
Defect GaAs	0.35	−2.8	0.03	Semiconductor (P)
Defective GaAs with aniline	0	0	0	Metallic
Defective GaAs with isoprene	0.78	−0.00023	0.78	Semiconductor (N)
Defective GaAs with o-toluidine	0	0	0	Metallic

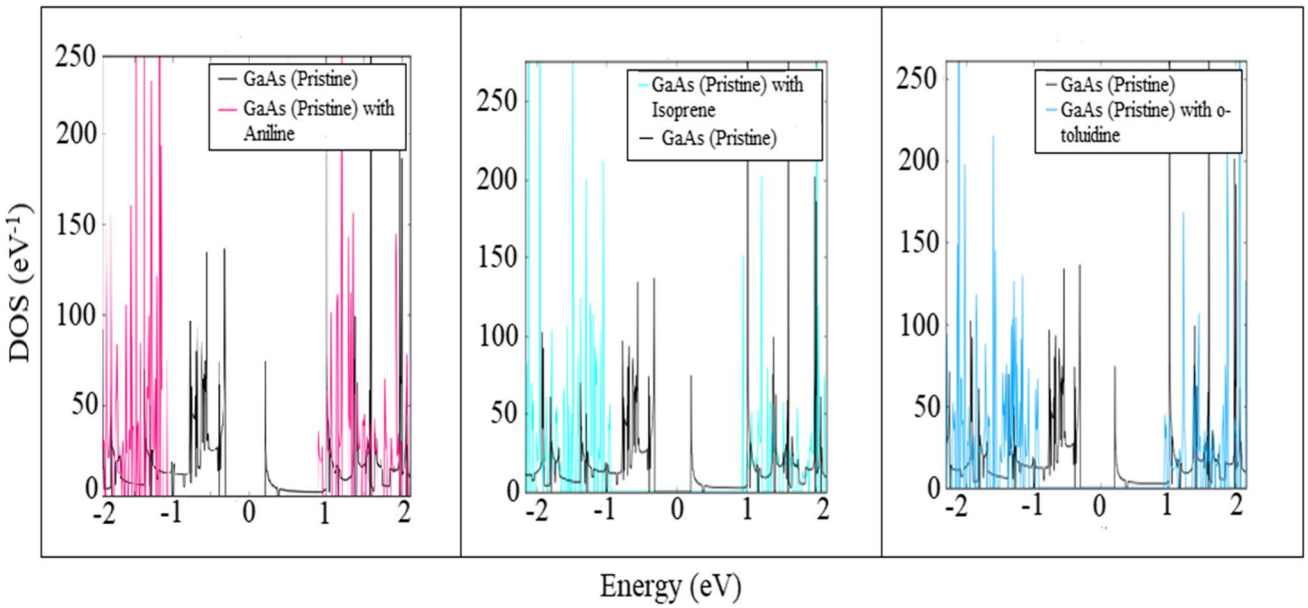

Fig. 7 DOS comparison of pristine GaAs with the adsorbed VOC analytes

energy levels of the traps or their number. The release of the trapped carriers is also dependent on the thermally activated process. Furthermore, when the analytes are adsorbed on the defective nanoribbon, there is complete redistribution of electrons producing entirely different energy states as opposed to the former ones. The DOS values range between − 2 and 2 eV, which corresponds to the bandgap of the complexes.

Electron density is a core property used in electronic structure (band structure and DOS) calculation via DFT calculations as effective potentials (Hartree, exchange–correlation and external potentials) are functional of electron density. It represents electron cloud or the probability function of an electron as function of distance. Figure 9 represents an iso-surface plot of the electron density calculated during electronic structure calculation for all 6 variants of GaAs-biomarker complex. It can be predicted from the observation that electron sharing occurs between the analytes and base materials.

To evaluate the transport properties, I-V characteristics of the GaAs nanoribbon are calculated. All I-V calculations are computed by adopting the two-probe model approach for the GaAs nanoribbon. Non-equilibrium Green's function (NEGF) calculations are applied, wherein first, the transmission coefficients are calculated as given in Eq. (2):

$$T(U) = tr(\mu_R F_C \mu_L F_C) \tag{2}$$

where $T(U)$ is the transmission coefficient, F_C is the Green's function and μ is the imaginary part of self-energy for left electrode if L subscript is used and right electrode if R subscript is used. Furthermore, the current $I(V)$ in the device is calculated as:

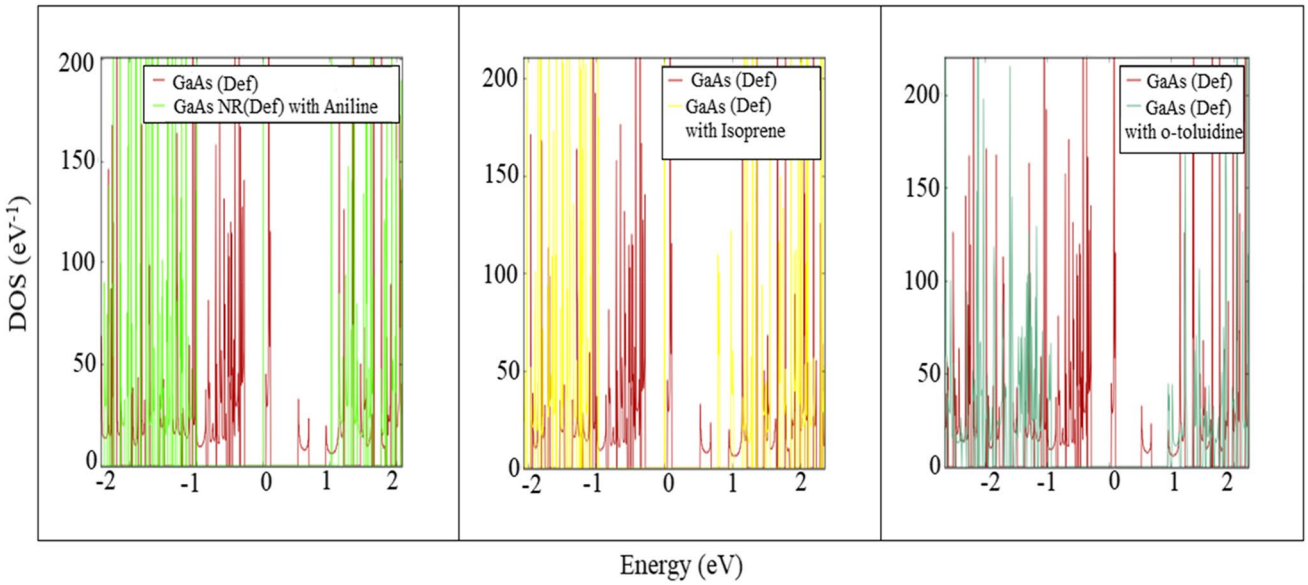

Fig. 8 DOS comparison of defective GaAs nanoribbon with the adsorbed VOC analytes

$$I(V) = \frac{2e}{h}\int_{\eta_L}^{\eta_R}\left(G\left(U-\eta_R\right) - G\left(U-\eta_L\right)T(U)\right)dU \tag{3}$$

Here, $\eta_R$and η_L are the chemical potentials of the electrode with respective notations. U notation is used for the energy. This requires the calculation of the Fermi–Dirac distribution as:

$$G(U-\eta) = \frac{1}{1+e^{\left(E-\frac{\eta}{K_B T_{temp}}\right)}} \tag{4}$$

swhere, K_B is the Boltzmann constant and T_{temp} is the temperature.

To use the proposed device as a biosensor for lung cancer in clinical research, the I-V characteristics in the presence and absence of the biomarker is calculated.

Figures 9 and 10 showcase that GaAs nanoribbon–based device exhibits negative differential resistance (NDR) characteristic as is shown by 1D and 2D graphene-like structured materials. The main reason behind the formation of this particular region is the ambipolar nature of materials [28] which states that after a particular voltage, like 1.8 V in pristine nanoribbon device (Fig. 9), the majority carriers (electrons or holes) are swept away from the device and conduction decreases until a point called valley point that is 2.1 V in pristine GaAs nanoribbon and then the holes outweigh and become the majority carrier in the device.

In comparison to IV characteristics in Figs. 9 and 10, it can observe that defective GaAs nanoribbon exhibits less peak current or current intensity as compared to the pristine one because of high electron–phonon scattering in defective GaAs nanoribbon, which deteriorates the mobility of the device as discussed in the starting of result and this section. However, adsorption of the biomarker decreases the current in pristine GaAs nanoribbon, which is even less than the current of biomarker-adsorbed defective GaAs nanoribbon because adsorption of biomarker molecules create more lattice distortion in pristine as compare to defective as shown in Figs. 3 and 4.

The formation of NDR region can also be treated as a sensing parameter for VOCs. In the case of pristine GaAs nanoribbon, only one NDR region is formed at 2.1 V. In contrast, adsorption of aniline, o-toluidine and isoprene forms three, four and two differential regions, respectively, up to 3.6 V. Creation of defect only causes a very low single NDR region up to 3.2 V. In contrast, aniline adsorption leads to the formation of 4 multi-valley NDR region up to 3.2 V which is much more effective in sensing as compared to pristine.

Another method for sensing molecules is through the calculation of peak current. For the pristine GaAs nanoribbon, it has been observed that the peak current decreases upon the adsorption of the VOC molecules. On the adsorption of o-toluidine on the GaAs nanoribbon, the current decreases 10^4 times which is a very minimal amount of current and hard to sense. It is also observed that the current remains constant up to the bias voltage of 2.4 V, and beyond this value, it abruptly increases. However, defective nanoribbon shows an increment in the peak current with adsorption of VOCs except for the isoprene, in which the current decreases with the adsorption process (Fig. 11). High peak currents are readily detectable in contrast to very low current variations. Therefore, defective nanoribbons show high current sensing performance as compared to the pristine counterpart.

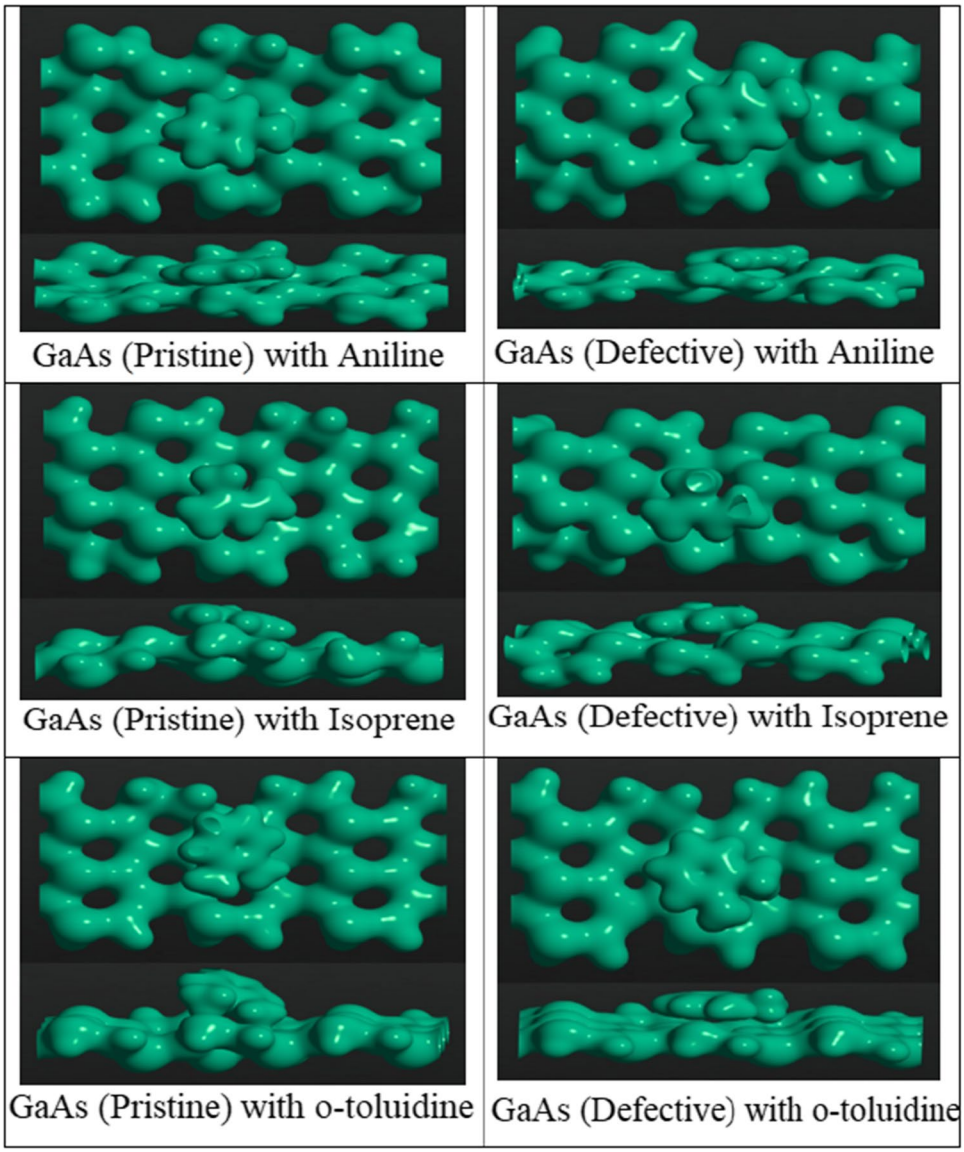

Fig. 9 Electron densities of pristine and defective GaAs nanoribbon with all three VOC analytes

Figures 12 and 13 show the transmission eigenstates calculated during transmission coefficient calculation discussed in Eq. (1) of the pristine and defective GaAs with all three analytes taken at a bias voltage of 0.6 V. Transmission eigenstates refer to the transmission matrix of eigenfunctions in real space. It represents the transmission probability of carriers in space. The transmission probability for the defective variants is higher than the pristine variants with adsorbed biomarker molecules**.**

Besides the use of GaAs nanoribbon as channel in a nanodevice sensor, it can also be used in the optical sensors. GaAs is said to be a very prominent optical material in diamond structure due to its direct bandgap nature which remains true in hexagonal shaped nanoribbon form as well. Therefore, it is better to explore the proposed nanoribbon's optical properties. The optical spectrum shows the peak of photon adsorption versus energy curve changes with the adsorption of the analyte. A material having distinct adsorption peaks reveals that they absorb different energies of photons, which leads to the designing of a photodetector-based sensor which absorbs different energies of photons upon adsorption of different molecules. In the case of pristine GaAs as shown in Fig. 14, peak is at 1.5 eV and the value of adsorption coefficient is around 70,000 cm^{-1}. After the adsorption of analytes, the peak shifted to 2.5 eV for all three analytes but with different adsorption coefficient of 7000, 15,000 and 10,000 cm^{-1} for aniline, isoprene and o-toluidine, respectively. It means albeit all three cases, the same photon energy is absorbed but the penetration depth inside is different, having the descending order as isoprene > o-toluidine > aniline. The introduction of the defect in the nanoribbon leads

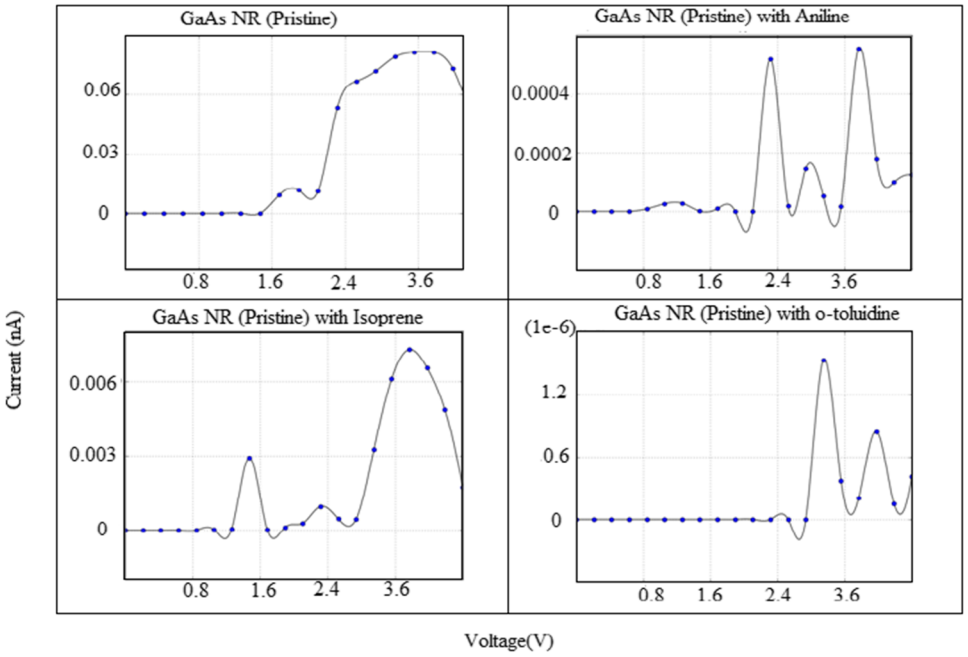

Fig. 10 I-V characteristics of pristine GaAs with all three VOC analytes

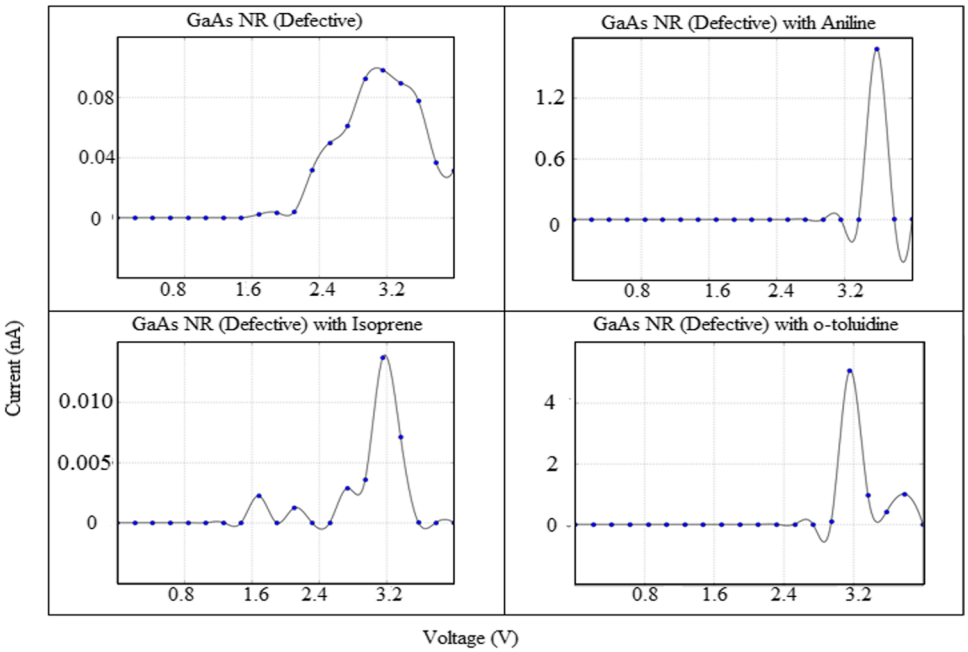

Fig. 11 I-V characteristics of defective GaAs with all three VOC analytes

to formation of three peaks in the optical spectrum with highest peak at 0.7 eV as shown in Fig. 15. This means defective material shows a broad range of absorption capabilities.

It changes to single peak spectrum after adsorption of the aniline. Adsorption of isoprene shifts the highest peak to 2.3 eV similar to o-toluidine. It shows that adsorption of analytes on defective nanoribbon not only changes the magnitude of adsorption coefficients but there are variations in the energies as well.

Conclusions

GaAs pristine and defected nanoribbons have been studied for their behaviour towards three different VOC biomarkers of lung cancer, aniline, isoprene and o-toluidine. Defective GaAs has shown the strongest interaction among the other structures as it has maximum value of the adsorption energy. Also, transport properties of the modelled device prove the same. The defect-induced nanoribbon has

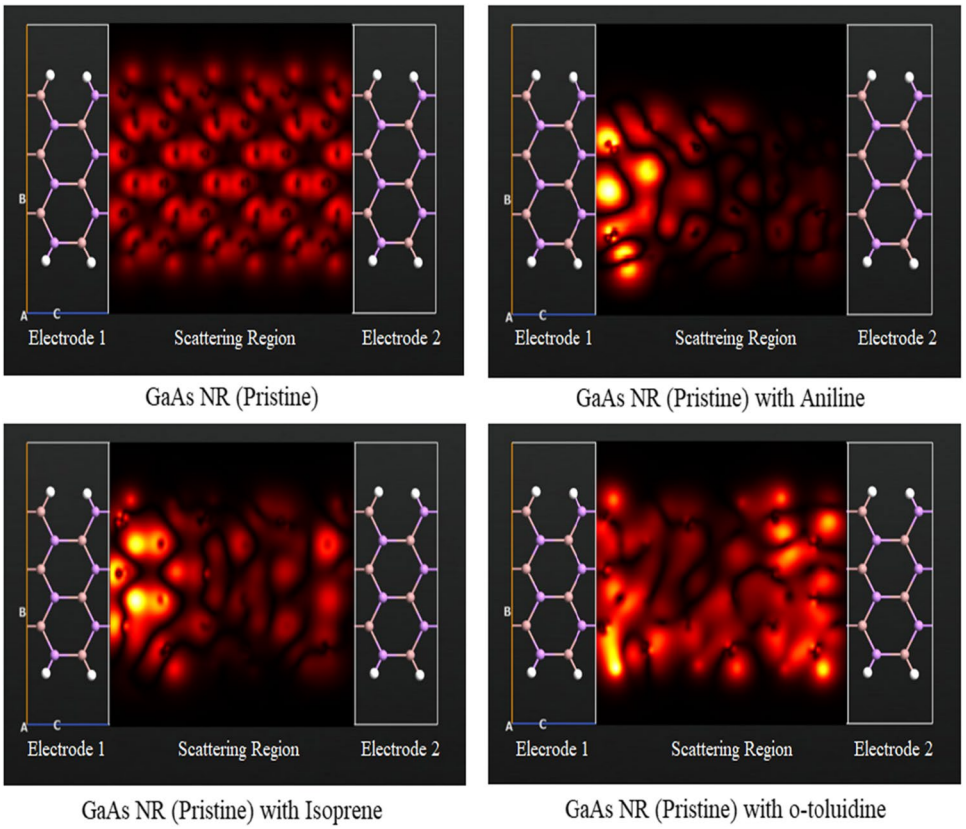

Fig. 12 Transmission eigenstates of pristine GaAs with all three analytes

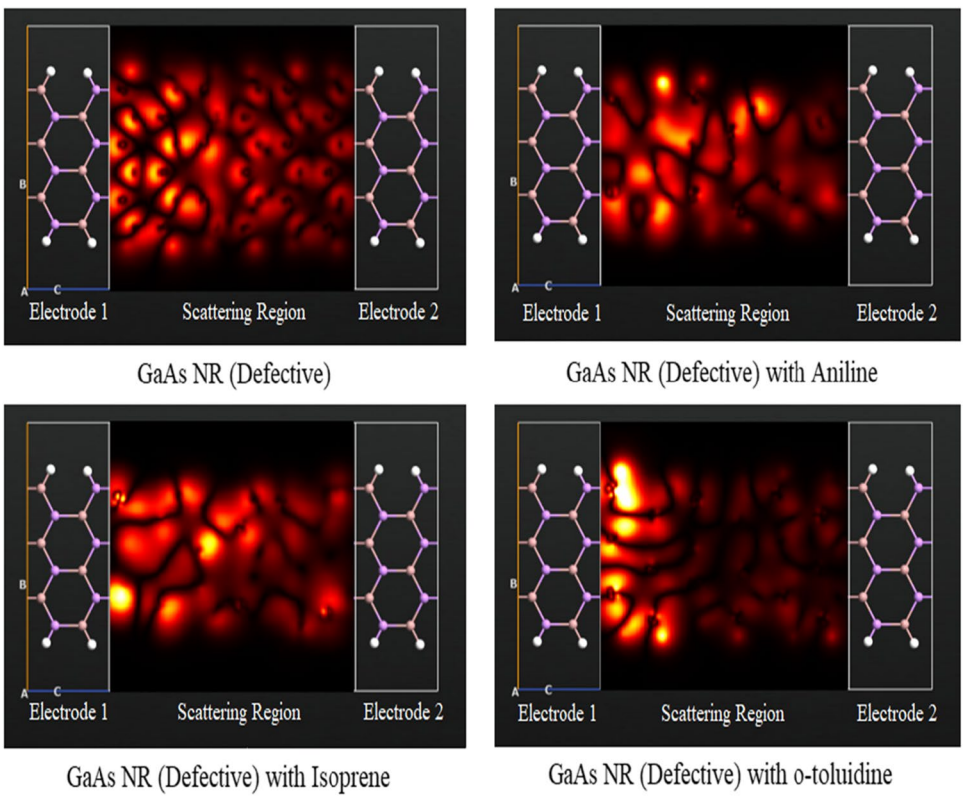

Fig. 13 Transmission eigenstates of defective GaAs with all three analytes

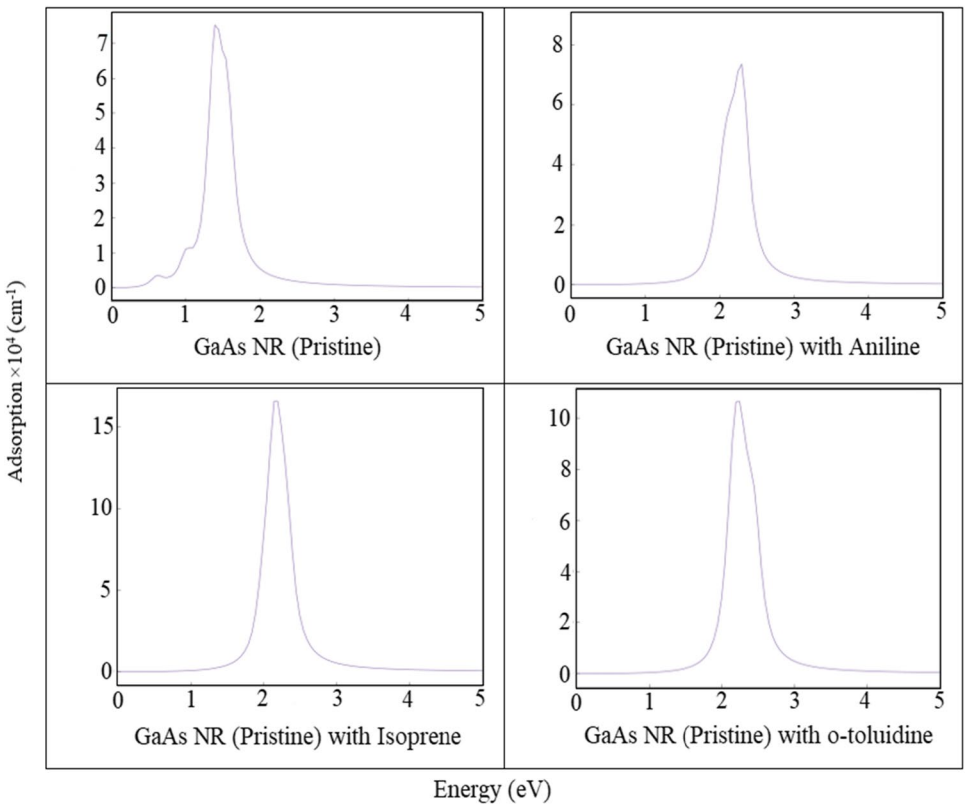

Fig. 14 Optical spectrums of pristine GaAs with all three analytes

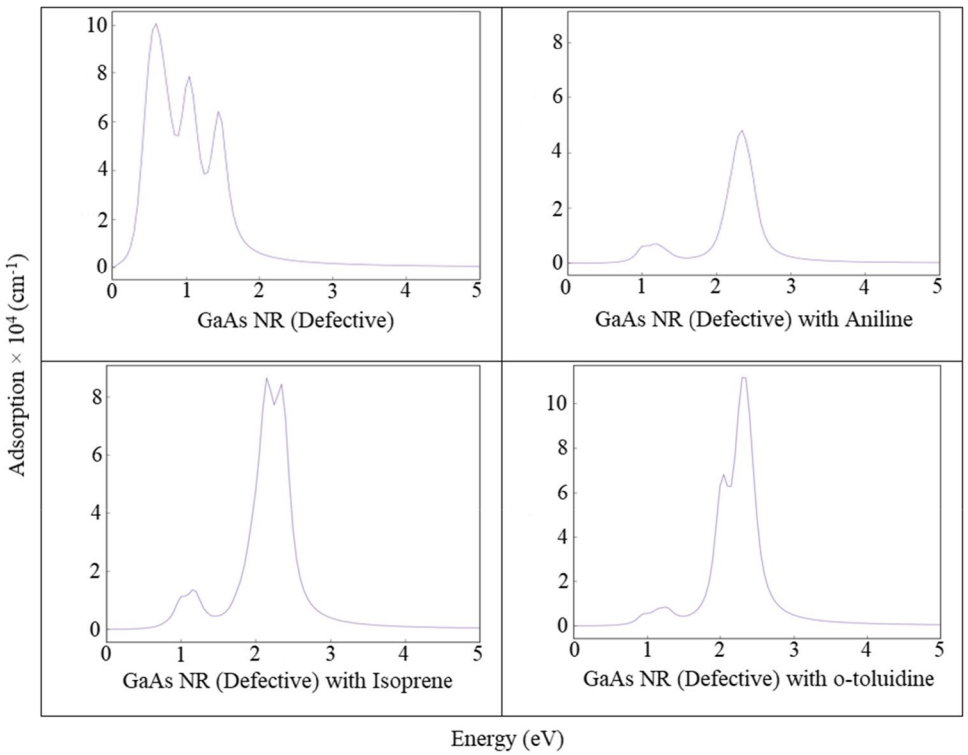

Fig. 15 Optical spectrums of defective GaAs with all three analytes

shown more adsorption in all three cases compared to the pristine nanoribbon. Also, it exhibits more conductivity as the band gap reduces to 0 eV in two cases after adsorption. Furthermore, the variation in the optical parameters in the case of defective nanoribbon is more; hence, it is more sensitive compared to the pristine nanoribbon. Although pristine GaAs has adsorbed the given analytes but the introduction of defects has improved the sensitivity of GaAs nanoribbons towards lung cancer detection.

Acknowledgements The authors are thankful to the National Institute of Technical Teachers Training and Research (NITTTR), Chandigarh, India, for permission to use Atomistix Toolkit (ATK) for the calculations.

Author contribution Not applicable.

Data availability Not applicable.

Code availability Not applicable.

Declarations

Ethics approval Not applicable.

Consent to participate Yes, all are ready to participate.

Consent for publication Yes, all are ready to publish.

Conflict of interest The authors declare no competing interests.

References

1. L. Dominioni, A. Imperatori, F. Rovera, A. Ochetti, G. Torrigiotti, M. Paolucci, Stage I nonsmall cell lung carcinoma, Cancer 89:2334.
2. Wan Q, Xu Y, Xiao H (2018) Exhaled gas detection by Ir-doped CNT for primary diagnosis of lung cancer. AIP Adv 8:105128. https://doi.org/10.1063/1.5050435
3. Pauling L, Robinson AB, Teranishi R, Cary P (1971) Quantitative analysis of urine vapor and breath by gas liquid partition chromatography. prOceedings of the National Academy of Sciences 68:2374. https://doi.org/10.1073/pnas.68.10.2374
4. Hoa LT, Tien HN, Luan VH, Chung JS, Hur SH (2013) Fabrication of a novel 2D-graphene/2D-NiO nanosheet-based hybrid nanostructure and its use in highly sensitive NO2 sensors. Sens Actuators, B Chem 185:701. https://doi.org/10.1016/j.snb.2013.05.050
5. Chen X-P, Wang L-M, Sun X, Meng R-S, Xiao J, Ye H-Y, Zhang G-Q (2017) Sulfur dioxide and nitrogen dioxide gas sensor based on arsenene: a first-principle study. IEEE Electron Device Lett 38:661. https://doi.org/10.1109/led.2017.2684239
6. Srimathi U, Nagarajan V, Chandiramouli R (2019) Germanane nanosheet as a novel biosensor for liver cirrhosis based on adsorption of biomarker volatiles – a DFT study. Appl Surf Sci 475:990. https://doi.org/10.1016/j.apsusc.2019.01.008
7. Aragay G, Pino F, Merkoçi A (2012) Nanomaterials for sensing and destroying pesticides. Chem Rev 112(10):5317–5338. https://doi.org/10.1021/cr300020c
8. Biju V (2014) Chemical modifications and bioconjugate reactions of nanomaterials for sensing, imaging, drug delivery and therapy. Chem Soc Rev 43(3):744–764. https://doi.org/10.1039/c3cs60273g
9. Demchenko AP, Dekaliuk MO (2013) Novel fluorescent carbonic nanomaterials for sensing and imaging. Methods and Applications in Fluorescence 1(4):042001. https://doi.org/10.1088/2050-6120/1/4/042001
10. Etienne M, Goux A, Sibottier E, Walcarius A (2009) Oriented mesoporous organosilica films on electrode: a new class of nanomaterials for sensing. J Nanosci Nanotechnol 9(4):2398–2406. https://doi.org/10.1166/jnn.2009.se39
11. Yoon HJ, Jun DH, Yang JH, Zhou Z, Yang SS, Cheng MM-C (2011) Carbon dioxide gas sensor using a graphene sheet. Sens Actuators, B Chem 157:310. https://doi.org/10.1016/j.snb.2011.03.035
12. Jeong HY, Lee D-S, Choi HK, Lee DH, Kim J-E, Lee JY, Lee W-J, Kim S-O, Choi S-Y (2010) Flexible room-temperature NO2 gas sensors based on carbon nanotubes/reduced graphene hybrid films. Appl Phys Lett 96(21):213105. https://doi.org/10.1063/1.3432446
13. Zheng Z, Wang H (2019) Different elements doped graphene sensor for CO2 greenhouse gases detection: the DFT study. Chem Phys Lett. https://doi.org/10.1016/j.cplett.2019.02.024
14. Shokuhi RA, Esfahanian M, Maleki S, Gharati G (2016) Application of carbon nanostructures toward SO2 and SO3adsorption: a comparison between pristine graphene and N doped graphene by DFT calculations. J Sulfur Chem 37(2):176–188. https://doi.org/10.1080/17415993.2015.1116536
15. Rad AS, Shabestari SS, Mohseni S, Aghouzi SA (2016) Study on the adsorption properties of O 3, SO 2, and SO 3 on B-doped graphene using DFT calculations. J Solid State Chem 237:204–210. https://doi.org/10.1016/j.jssc.2016.02.023
16. Walia GK, Randhawa DKK (2017) Electronic and transport properties of silicene-based ammonia nanosensors: an ab initio study. Struct Chem 29:257. https://doi.org/10.1007/s11224-017-1025-9
17. Walia GK, Randhawa DKK (2018) First-principles investigation on defect-induced silicene nanoribbons — a superior media for sensing NH 3, NO 2 and NO gas molecules. Surf Sci 670:33. https://doi.org/10.1016/j.susc.2017.12.013
18. Walia, G. K., & Randhawa D. K. K. (2018). Adsorption and dissociation of sulfur-based toxic gas molecules on silicene nanoribbons: a quest for high-performance gas sensors and catalysts. Journal of Molecular Modeling, 24(4).https://doi.org/10.1007/s00894-018-3631-x
19. Walia GK, Randhawa DKK (2018) Gas-sensing properties of armchair silicene nanoribbons towards carbon-based gases with single-molecule resolution. Struct Chem 29:1893. https://doi.org/10.1007/s11224-018-1170-9
20. Walia GK, Randhawa DKK (2018) Density-functional study of hydrogen cyanide adsorption on silicene nanoribbons. J Mol Model 24:242. https://doi.org/10.1007/s00894-018-3782-9
21. Sadeghi H, Bailey S, Lambert CJ (2014) Silicene-based DNA nucleobase sensing. Appl Phys Lett 104(10):103104. https://doi.org/10.1063/1.4868123
22. Tarun, T., Randhawa, D. K. K., Singh, P., Choudhary, B. C., Walia, G. K., & Kaur, N. (2020). Analysis of uric acid adsorption on armchair silicene nanoribbons: a DFT study. Journal of Molecular Modeling, 26(3).https://doi.org/10.1007/s00894-020-4313-z
23. Singh, P., Randhawa, D. K. K., Tarun, Choudhary, B. C., Walia, G. K., & Kaur, N. (2019). First principles investigation on armchair zinc oxide nanoribbons as uric acid sensors. Journal of Molecular Modeling, 26(1).https://doi.org/10.1007/s00894-019-4243-9
24. Kou L, Li C, Zhang Z, Guo W (2010) Tuning magnetism in zigzag ZnO nanoribbons by transverse electric fields. ACS Nano 4(4):2124–2128. https://doi.org/10.1021/nn901552b

25. Topsakal, M., Cahangirov, S., Bekaroglu, E., & Ciraci, S. (2009). First-principles study of zinc oxide honeycomb structures. Physical Review B, 80(23).https://doi.org/10.1103/physrevb.80.235119
26. Xia W, Hu W, Li Z, Yang J (2014) A first-principles study of gas adsorption on germanene. Phys Chem Chem Phys 16:22495. https://doi.org/10.1039/c4cp03292f
27. Monshi MM, Aghaei SM, Calizo I (2017) Doping and defect-induced germanene: a superior media for sensing H 2 S, SO 2, and CO 2 gas molecules. Surf Sci 665:96. https://doi.org/10.1016/j.susc.2017.08.012
28. Nagarajan V, Chandiramouli R (2017) NO 2 adsorption behaviour on germanene nanosheet – a first-principles investigation. Superlattices Microstruct 101:160. https://doi.org/10.1016/j.spmi.2016.11.032
29. Nagarajan V, Chandiramouli R (2017) CO and NO monitoring using pristine germanene nanosheets: DFT study. J Mol Liq 234:355. https://doi.org/10.1016/j.molliq.2017.03.100
30. Choi S-J, Kim I-D (2018) Recent developments in 2D nanomaterials for chemiresistive-type gas sensors. Electron Mater Lett 14:221. https://doi.org/10.1007/s13391-018-0044-z
31. Rozahun I, Bahti T, He G, Ghupur Y, Ablat A, Mamat M (2018) GaAs monolayer: Excellent SHG responses and semi metallic to metallic transition modulated by vacancy effect. Appl Surf Sci 441:401. https://doi.org/10.1016/j.apsusc.2018.02.045
32. Volovik BV, Kovsh AR, Passenberg W, Kuenzel H, Grote N, Cherkashin NA, Ustinov VM (2001) Optical and structural properties of self-organized InGaAsN/GaAs nanostructures. Semicond Sci Technol 16(3):186–190. https://doi.org/10.1088/0268-1242/16/3/312
33. Liang D, Huo Y, Kang Y, Wang KX, Gu A, Tan M, Yu Z, Li S, Jia J, Bao X, Wang S, Yao Y, Wong HS, Fan S, Cui Y, Harris JS (2012) Optical absorption enhancement in freestanding gaas thin film nanopyramid arrays. Adv Energy Mater 2(10):1254–1260. https://doi.org/10.1002/aenm.201200022
34. Rouzhahong, Y., Wushuer, M., Mamat, M., Wang, Q., & Wang, Q. (2020). First principles calculation for photocatalytic activity of GaAs Monolayer. Scientific Reports, 10(1).https://doi.org/10.1038/s41598-020-66575-9
35. Şahin, H., Cahangirov, S., Topsakal, M., Bekaroglu, E., Akturk, E., Senger, R. T., & Ciraci, S. (2009). Monolayer honeycomb structures of group-IV elements and III-V binary compounds: first-principles calculations. Physical Review B, 80(15).https://doi.org/10.1103/physrevb.80.155453
36. Synopsys QuantumATK (https://www.synopsys.com/silicon/quantumatk.html)
37. Wu Y, Farmer DB, Zhu W, Han SJ, Dimitrakopoulos CD, Bol AA, Avouris P, Lin YM (2012) Three-terminal graphene negative differential resistance devices. ACS Nano 6(3):2610–2616. https://doi.org/10.1021/nn205106z